International Journal of Numerical Methods for Heat & Fluid Flow
Simulation of laminar confined flow past a circular cylinder with integral wake splitter involving heat transfer
B.S.V.P. PatnaikK.N. SeetharamuP.A. Aswatha Narayana

Article information:

For Authors

If you would like to write for this, or any other Emerald publication, then please use our Emerald for Authors service information about how to choose which publication to write for and submission guidelines are available for all. Please visit www.emeraldinsight.com/authors for more information.

About Emerald www.emeraldinsight.com

Emerald is a global publisher linking research and practice to the benefit of society. The company manages a portfolio of more than 290 journals and over 2,350 books and book series volumes, as well as providing an extensive range of online products and additional customer resources and services.

Emerald is both COUNTER 4 and TRANSFER compliant. The organization is a partner of the Committee on Publication Ethics (COPE) and also works with Portico and the LOCKSS initiative for digital archive preservation.

*Related content and download information correct at time of download.

SIMULATION OF LAMINAR CONFINED FLOW PAST A CIRCULAR CYLINDER WITH INTEGRAL WAKE SPLITTER INVOLVING HEAT TRANSFER

B.S.V.P. PATNAIK†, K.N. SEETHARAMU‡ AND P.A. ASWATHA NARAYANA†

†*Department of Applied Mechanics*
‡*Department of Mechanical Engineering*
Indian Institute of Technology, Madras-600 036, India

ABSTRACT

A finite element method is used to study the effect of flow past a circular cylinder with an integral wake splitter. A fractional step algorithm is employed to solve the Navier-Stokes and Energy equations with a Galerkin weighted residual formulation. The vortex shedding process is simulated and the effect of splitter addition on the time period of shedding is studied at a Reynolds number of 200 and a blockage ratio of 0.25. The effect of splitter and the Strouhal number and heat transfer augmentation per unit pressure drop has been investigated.

KEY WORDS   Heat transfer augmentation   Strouhal number   Vortex shedding   Wake splitters

NOMENCLATURE

BR	= Blockage ratio (D/H)	SPL	= Splitter plate length
D	= Cylinder diameter	St	= Strouhal number ($f_{vs}*D/U_{av}$)
f_{vs}	= Frequency of vortex shedding	T	= Temperature
$FDPV$	= Fully developed parabolic velocity	T_{ps}	= Time period of shedding
H	= Height of the channel	U_{av}	= Average velocity
$IWSP$	= Integral wake splitter plate	U	= Non-dimensionalized velocity in x-direction
k	= Thermal conductivity of the fluid	V	= Non-dimensionalized velocity in y-direction
Nu	= Nusselt number ($\partial T/\partial Y|_{wall}$)	ψ	= Non-dimensional stream function
P	= Non-dimensional pressure	ς	= Non-dimensional vorticity
Pr	= Prandtl number (v/α)	τ	= Non-dimensional time
Re	= Reynolds number ($U_{av}*D/v$)	Δ	= Difference operator
S	= Distance measured along the cylinder and splitter surface	n	= At the nth time step
		v	= Kinetic viscosity
L	= Length of the integral wake splitter	α	= Thermal diffusivity
$SEVP$	= Stabilized error vector propagator		

INTRODUCTION

Flow past a circular cylinder is a challenging, basic and fundamental fluid mechanics problem and has wide engineering applications. The highly asymmetric and periodic nature of the flow in the downstream has attracted the attention of physicists and engineers alike. From the physics point of view, it is highly fascinating to understand how and why such a highly symmetric flow in the upstream becomes so highly asymmetric in the downstream.

A circular cylinder can be seen as a part of a tube bundle in diverse engineering applications such as heat exchangers, air conditioning coils, nuclear reactor fuel rods, etc. In many situations gas flow over the tubes has a permissible gas side pressure drop. This restricts the power of the

blower or pump being used. Gases, because of their high thermal resistances, give a low heat transfer coefficient. To make the heat exchanger economical, it is required that heat transfer per unit pressure drop be higher. To achieve this objective extended surfaces, vortex generators, oval or flattened tubes are usually used. A noble approach is by the use of splitter plates.

Around Reynolds numbers of 40, the two stationary Föppal vortices are shed downstream. Vortex shedding from the circular body results in flow-induced vibration, which is characterized by Strouhal number. When a relation for Reynolds number (*Re*) against Strouhal number (*St*) is plotted for a circular cylinder, a peak can be noticed in the 200 to 300 *Re* range as shown by Blevins[1]. Zdrakovich[2] and Aref and Siggia[3] attribute the shedding process to the instability caused by the sinuous motions in the far wake. On the other hand, Perry *et al.*[4] have proposed a different mechanism known as the instantaneous "alley-way" concept. This idea had the support of Gresho *et al.*[5] as well as Sa and Chang[6] subsequently. In simulating the flow past a square cylinder, Kelkar and Patankar[7] have applied numerical perturbation to simulate the vortex shedding in an infinite medium. The blockage ratio effect in confinement has been investigated by Ökajima[8], Mukhopadhyay *et al.*[9].

The Reynolds numbers associated with these flows are sufficiently high to produce turbulence *in the wake region. Slaouti and Stansby[10], point out that there is no general turbulence model to* incorporate into the numerical simulation of unsteady separated flows. Though direct numerical simulation is possible, present day computing power requirements prohibit the direct three-dimensional simulation of Navier-Stokes equations. It has been observed in the experiments of Slaouti and Gerrard[11], that some concepts of large-scale wake behaviour associated with vortex shedding at high Reynolds numbers (greater than 10^4) are similar to the flow at low Reynolds numbers (100-200). For low Reynolds numbers, the flow and forces acting on the circular cylinder can very well be predicted by two-dimensional laminar computations.

Roshko[12] was the first to demonstrate that vortex shedding is fully inhibited by the addition of a splitter plate of length 4-5 times the cylinder diameter. Since then, systematic studies have been made by Roshko[13], Bearman[14], Gerrard[15], Apelt and West[16]. Heat transfer aspects have been studied by Sparrow and Kang[17] and Ibrahim[18].

Flow visualization plays a vital role in the basic understanding of the flow phenomena and also provides a physical intuitive reasoning. It has also been noticed that the computer laboratory lags far behind, in the race of offering basic understanding of flow physics and heat transfer by means of flow visuals (snapshots taken by flow visualization techniques). This gives ample scope for the need to generate numerical flow visuals by way of simulation. Though a good number of interesting experimental papers do exist on integral wake splitter plates, to the knowledge of the authors not a single paper has been published using numerical computations. This prompted us to set the objectives of the present paper as to simulate numerically and validate the time evolution of flow past a circular cylinder in a channel and study the effect of adding a wake splitter in the downstream, integral with the cylinder. The influence of triangular and rectangular wake splitters for lengths 0.25D, 0.5D and 1.0D have been studied.

METHOD OF ANALYSIS

Analysis is essentially based on the explicit time integration of Navier-Stokes equations, which is based on the projection scheme originally developed by Chorin[19] in a finite difference context. This has been extended to finite element laminar flow problems by Donea *et al.*[20]. This algorithm, along with Galerkin weighted residual formulation, has been used in the finite element method to solve full Navier-Stokes equations (1) through (3) after the following non-dimensionalization.

$$X = x/D \; ; Y = y/D \; ; U = u/U_{av} \; ; V = v/U_{av}$$

$$\tau = t * U_{av}/D \; ; P = p/\rho U_{av}^2 \text{ and } T = T*/T_{ref}$$

Where D, is the cylinder diameter U_{av} is the average velocity in the channel and T_{ref} corresponds to the reference temperature.

$$\frac{\partial U}{\partial X} + \frac{\partial V}{\partial Y} = 0 \tag{1}$$

$$\frac{\partial U}{\partial \tau} + U\frac{\partial U}{\partial X} + V\frac{\partial U}{\partial Y} = -\frac{\partial P}{\partial X} + \frac{1}{Re}\left[\frac{\partial^2 U}{\partial X^2} + \frac{\partial^2 U}{\partial Y^2}\right] \tag{2}$$

$$\frac{\partial V}{\partial \tau} + U\frac{\partial V}{\partial X} + V\frac{\partial V}{\partial Y} = -\frac{\partial P}{\partial Y} + \frac{1}{Re}\left[\frac{\partial^2 V}{\partial X^2} + \frac{\partial^2 V}{\partial Y^2}\right] \tag{3}$$

$$\frac{\partial T}{\partial \tau} + U\frac{\partial T}{\partial X} + V\frac{\partial T}{\partial Y} = \frac{1}{Re*Pr}\left[\frac{\partial^2 T}{\partial X^2} + \frac{\partial^2 T}{\partial Y^2}\right] \tag{4}$$

The solution algorithm employed in the present study is an Eulerian velocity correction method which is also known as fractional step algorithm. In each time step of the algorithm, the following three steps are repeated.

(1) Calculation of pseudo velocities.
(2) Evaluating pressure from pressure Poisson equation.
(3) Correcting the pseudo velocities to get actual velocities.

Heat is treated as a passive scalar, and the energy equation is solved to obtain the temperature distribution. In this case also the Galerkin formulation is applied.

As per step (1), the pressure term is dropped from X and Y momentum equations (2) and (3) and the pseudo (fictitious) velocities are calculated. Modified X momentum equation is as shown in (5). The velocities are so named because they will not satisfy the continuity equation.

$$\frac{\partial \bar{U}}{\partial \tau} = -\left[U\frac{\partial U}{\partial X} + V\frac{\partial U}{\partial Y}\right] + \frac{1}{Re}\left[\frac{\partial^2 U}{\partial X^2} + \frac{\partial^2 U}{\partial Y^2}\right] \tag{5}$$

Expanding the left hand side of (5) by Euler's explicit scheme of forward differencing yields,

$$\frac{\partial \bar{U}}{\partial \tau} = \frac{\bar{U}^{n+1} - \bar{U}^n}{\Delta \tau^n} \tag{6}$$

Equating equations (5) and (6) the following equation is obtained.

$$\bar{U}^{n+1} = \bar{U}^n + \Delta\tau^n\left\{-\left[U\frac{\partial U}{\partial X} + V\frac{\partial U}{\partial Y}\right] + \frac{1}{Re}\left[\frac{\partial^2 U}{\partial X^2} + \frac{\partial^2 U}{\partial Y^2}\right]\right\} \tag{7}$$

Proceeding on the same lines, the Y momentum equation (3), takes the following form.

$$\bar{V}^{n+1} = \bar{V}^n + \Delta\tau^n\left\{-\left[U\frac{\partial V}{\partial X} + V\frac{\partial V}{\partial Y}\right] + \frac{1}{Re}\left[\frac{\partial^2 V}{\partial X^2} + \frac{\partial^2 V}{\partial Y^2}\right]\right\} \tag{8}$$

When the pressure term which was ignored is added,

$$\frac{\partial U}{\partial \tau} = -\frac{\partial P}{\partial X} + \frac{\partial \bar{U}}{\partial \tau} \tag{9}$$

$$\Rightarrow \frac{U^{n+1} - U^n}{\Delta\tau^n} = -\frac{\partial P^{n+1}}{\partial X} + \frac{\bar{U}^{n+1} - U^n}{\Delta\tau^n}.$$

On excluding common terms on both the sides,

$$\Rightarrow \frac{\partial P^{n+1}}{\partial X} = \frac{\bar{U}^{n+1} - U^{n+1}}{\Delta \tau^n} \tag{10}$$

$$\Rightarrow U^{n+1} = \bar{U}^{n+1} - \Delta \tau^n \frac{\partial P^{n+1}}{\partial X}. \tag{11}$$

Proceeding on similar lines, (13) is obtained.

$$\frac{\partial P^{n+1}}{\partial Y} = \frac{\bar{V}^{n+1} - V^{n+1}}{\Delta \tau^n} \tag{12}$$

$$\Rightarrow \bar{V}^{n+1} = \bar{V}^{n+1} - \Delta \tau^n \frac{\partial P^{n+1}}{\partial X}. \tag{13}$$

The summation after taking derivative with respect to X for equation (10) and Y derivative for equation (12) yields the pressure Poisson equation (14), which is solved for pressures:

$$\frac{\partial^2 P^{n+1}}{\partial X^2} + \frac{\partial^2 P^{n+1}}{\partial Y^2} = \frac{1}{\Delta \tau^n} \left[\frac{\partial \bar{U}^{n+1}}{\partial X} + \frac{\partial \bar{V}^{n+1}}{\partial Y} \right]. \tag{14}$$

The finite element spatial discretization is performed by the Galerkin weighted residual formulation, where the shape function itself is the weighting function. Linear triangular elements are used to represent U, V, P and T which are approximated as

$$\begin{aligned}
U &= N_i U_i + N_j U_j + N_k U_k, \\
V &= N_i V_i + N_j V_j + N_k V_k, \\
P &= N_i P_i + N_j P_j + N_k P_k, \\
T &= N_i T_i + N_j T_j + N_k T_k.
\end{aligned} \tag{15}$$

Details of the formulation are as in Fletcher[21] and the shape functions given by (14) defined for the triangular elements are as in Segarlind[22].

By obtaining the velocity field a priori, the following stream function equation (16) is solved with appropriate boundary conditions to obtain the ψ values.

$$\frac{\partial^2 \psi}{\partial X^2} + \frac{\partial^2 \psi}{\partial Y^2} = - \left[\frac{\partial V}{\partial X} - \frac{\partial U}{\partial Y} \right] \tag{16}$$

RESULTS AND DISCUSSION

Flow past an isothermal circular cylinder of diameter (D) is numerically simulated at a Reynolds number of 200 in a channel of height $4D$. This results in a blockage ratio (BR) of 0.25. A splitter plate is attached integral with the cylinder (known as cylinder with integral wake splitter plate) and is shown in *Figure 1*, its corresponding flow domain is given in *Figure 2*. No-slip boundary condition is applied for the cylinder, splitter surface and channel walls. For pressure, the homogeneous Neumann boundary condition is naturally incorporated, with a traction free exit. First order boundary conditions are specified at the channel exit. *Figure 3* shows the corresponding finite element mesh.
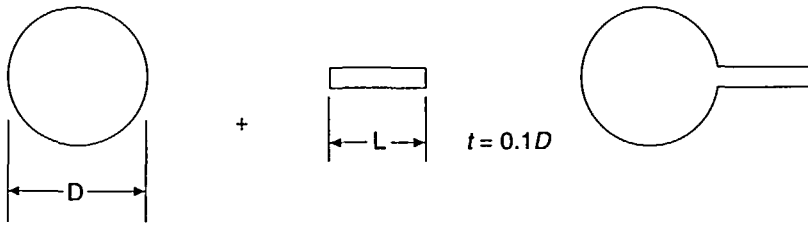
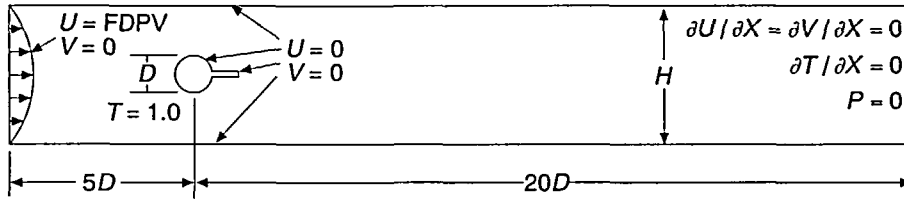*Figure 1*   Configurations of cylinder, splitter and combined

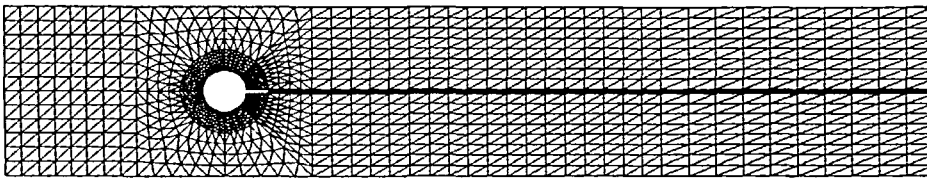*Figure 2*   Cylinder with an IWSP located in a channel

Figure 3   Finite element mesh for the configuration of cylinder with an IWSP of 0.5D in length

VORTEX SHEDDING FROM THE CYLINDER

Streamlines corresponding to the flow past a circular cylinder is shown in *Figure 4*. Here, initially, as in *Figure 4(a)* the flow is symmetric. At time (τ) = 1.22, incipience of separation results as in *Figure 4(b)*. The formation of two symmetric attached eddies of opposite vorticity can be noticed in *Figure 4(c)*. These eddies are fed by circulation from the shear layers and grow in size. The eddy growth with time can be seen in *Figure 4(d)*. The symmetric standing eddies attached to the cylinder surface have an "alley-way" passage for flow penetration. Flow penetrates either from the top or from the bottom into the "alley-way" the so-called narrow passage. The eddies become weak and symmetry is lost at τ = 17.6, as in *Figure 4(e)*. The eddy about to be washed away in the wake can be seen in *Figure 4(f)* at τ = 20.4.

With further progress in time, the eddy shedding periods are established. Initially eddies are longer and hence the eddy formation region is larger. With time it becomes tighter and closer to the formation region. Mukhopadyay[23], has shown that the time evolution of lift coefficient and monitored velocity both gave an identical period of shedding (T_{ps}). At *BR* = 0.25 for a Reynolds numbers of 200, the eddy is fully formed at the bottom and a sinuous motion can be seen in the downstream as in the numerical visual in *Figure 5(a)*. This creates a wake cavity on the top side. Flow entrains through this wake cavity and the vortex gets folded up as in *Figure 5(b)*. This eddy is subsequently shed. With further progress of time, eddy formation on the top side takes place, as can be seen in *Figure 5(c)* at τ = 42.1. *Figure 5(d)* shows a fully grown eddy on the top. It should be noted here that *Figures 5(a)* and *5(d)* visually represent flow pattern at half shedding cycle apart. Once two vortices are shed (one from the top and another from the bottom) one shedding cycle is completed. Again a new cycle starts and the periodic process continues.
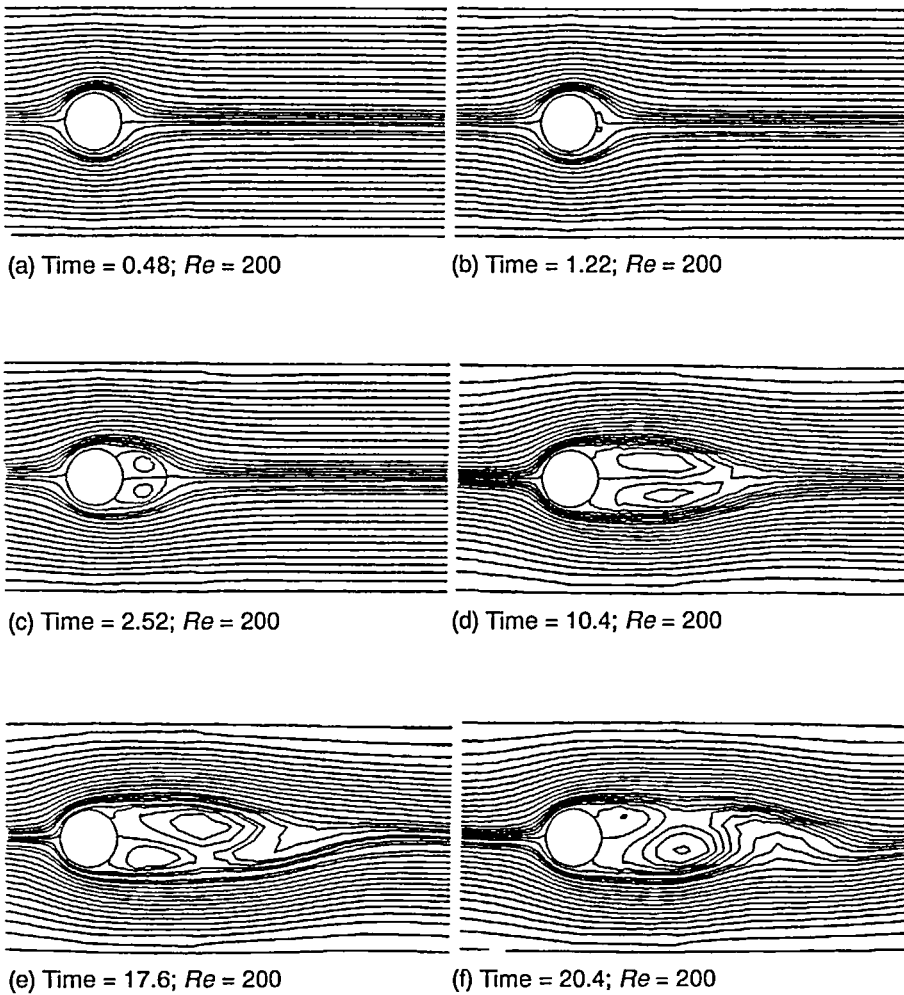
(a) Time = 0.48; *Re* = 200　　(b) Time = 1.22; *Re* = 200

(c) Time = 2.52; *Re* = 200　　(d) Time = 10.4; *Re* = 200

(e) Time = 17.6; *Re* = 200　　(f) Time = 20.4; *Re* = 200

Figure 4　Time evolution of streamlines for flow past a circular cylinder with *BR* = 0.25 and *Re* = 200

Son and Hanratty[24], suggest that to simulate vortex shedding, asymmetric disturbance in the upstream is required. But in a physical situation, the process is so natural and is hailed by the multiple perturbation sources such as non-uniform inlet conditions, surface roughness, perturbations in running conditions of the experiments etc., which could lead to destruction of the symmetry of the eddies. Though Kelkar and Patankar[7] have applied numerical perturbations to initiate shedding, in an earlier paper Braza *et al.*[25] have pointed out that the truncation and round off errors, and errors due to numerical approximations act as perturbating factors and eventually generate vortex shedding.

Figure 6 gives the monitored velocity against time for the above case, which shows no fluctuations up to τ = 20.4. Above this a regular, periodic fluctuation has been noticed. The time period of shedding has been marked in the figure. It should be stated that the two circled points on the top and bottom correspond to *Figure 5(a)* and *Figure 5(d)*, which are at half shedding cycle apart.
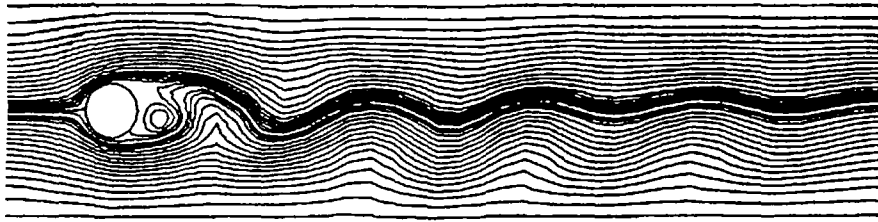
(a) Time = 40.61; *Re* = 200
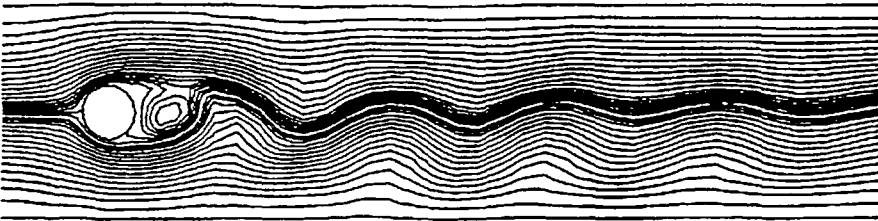
(b) Time = 41.20; *Re* = 200
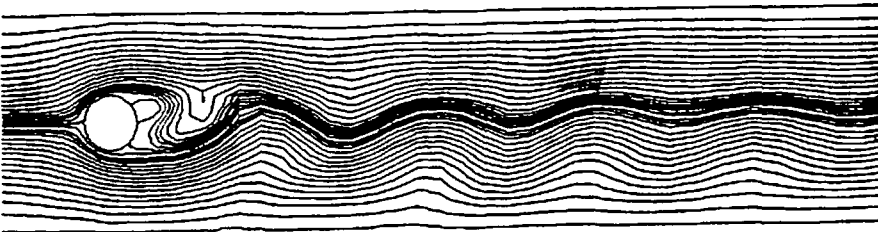
(c) Time = 42.10; *Re* = 200
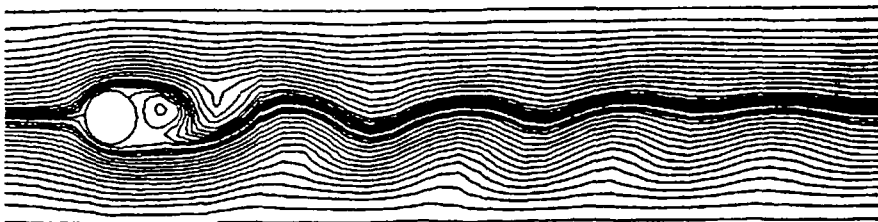
(d) Time = 42.80; *Re* = 200

Figure 5   Streamlines half shedding cycle apart at *Re* = 200 and *BR* = 0.25. (a) Vortex at the bottom; (b) Vortex folded up; (c) Formation of vortex at the top; (d) Fully grown vortex at the top

PRODUCTION OF VORTICITY ON THE CYLINDER

Vorticity is the curl of the velocity vector and is given as $\varsigma = \nabla \times \vec{V}$. *Figure 7* shows the time evolution of isovorticity contours for flow past a circular cylinder, at *BR* = 0.25 and *Re* = 200. It can be noticed that two thin vortex layers symmetrically situated, leave the surface of the cylinder and curl round themselves. Vorticity becomes more and more concentrated in the rolled up
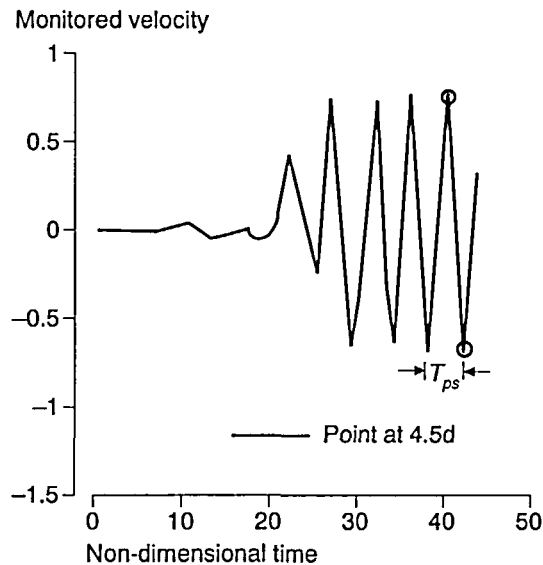
Monitored velocity

Figure 6   Signal traces of the monitored velocity

portions. *Figure 7(c)* shows the elongation of vortices which signifies increasing strength and they move away from the cylinder. *Figure 7(d)* shows as to how the constant vorticity lines become longer and longer in the flow direction. Meanwhile each vortex produces a strong back flow on the rear of the cylinder. Gerrard[15] points out that after reaching sufficient concentration, a further supply of circulation to the vortex is cut off. Hence, elongated vortices cease to increase in strength. We may speak of the vortex being shed from the body at this stage. The karman vortex street can be seen in *Figure 7(e)* and *7(f)*, which are at half shedding cycle apart.

STROUHAL NUMBER CALCULATION

Strouhal number *(St)* represents a measure of the oscillating fluid flow phenomenon. It is defined as the ratio of the product of vortex shedding frequency (f_{vs}) and cylinder diameter (D) to the free stream velocity (U_∞). When "U_∞" and "D" are non-dimensionalized as unity, "St" simply equals "f_{vs}". The vortex shedding frequency "f_{vs}" is obtained as the inverse of the time period of shedding (T_{ps}). *Table 1* gives the Strouhal number comparison for an infinite medium. The Strouhal number at $BR = 0.25$ is 0.255, corresponding to a time period of shedding equal to 3. 917.

The present results are in good agreement especially with the experimental results of Gerrard[15] and Roshko[13] in addition to the numerical results of Gresho *et al.,*[5] Karniadakis[26] and Sa and Chang[6].

DETERMINATION OF NUSSELT NUMBER

A knowledge of heat transfer coefficient at low Reynolds numbers is also valuable in the development of instruments using wires such as thermo elements and hot wire anemometers[27]. Here the parameter of interest is the Nusselt number. In order to obtain the temperature distribution in the flow domain, the energy equation is solved after solving the N-S equations. The local Nusselt numbers are obtained by calculating the temperature gradient on the surface of the circular cylinder. i.e.
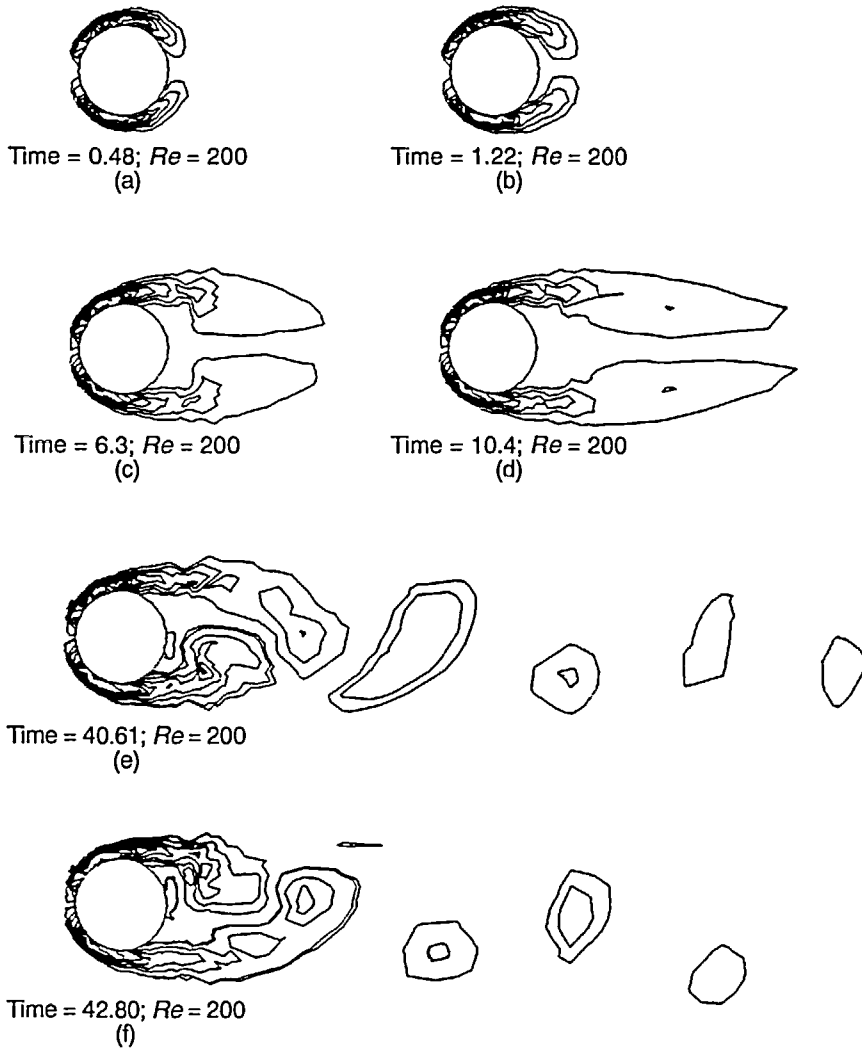
$$Nu_{local} = \left. \frac{\partial T}{\partial Y} \right|_{wall}$$

Time = 0.48; *Re* = 200
(a)

Time = 1.22; *Re* = 200
(b)

Time = 6.3; *Re* = 200
(c)

Time = 10.4; *Re* = 200
(d)

Time = 40.61; *Re* = 200
(e)

Time = 42.80; *Re* = 200
(f)

Figure 7   Time evolution of vorticity contours

Table 1   Comparison of Reynolds number with Strouhal number

| Source | Reynolds number | | |
| | 50 | 100 | 200 |
	Strouhal number (*St*)		
Gerrard[15] (Experimental)	–	0.16	0.18-0.20
Roshko[13] (Experimental)	0.14	0.16	0.17-0.19
Gresho et al.[5] (Numerical)	0.14	0.18	0.21
Karniadakis[26] (Spectral)	0.14	0.18	0.20
Sa and Chang[6] (SEVP)	–	0.155	0.186
Present study	0.139	0.154	0.192

In *Figure 8* the local Nusselt number distribution of an isothermal cylinder in an infinite medium at *Re* = 200 has been compared with the experimental results of Eckert and Soehngen[27] and finite difference results of Chun and Boehm[28]. Because the thermal boundary layer growth

Local Nusselt number

Key
················ Eckert's experimental [27]
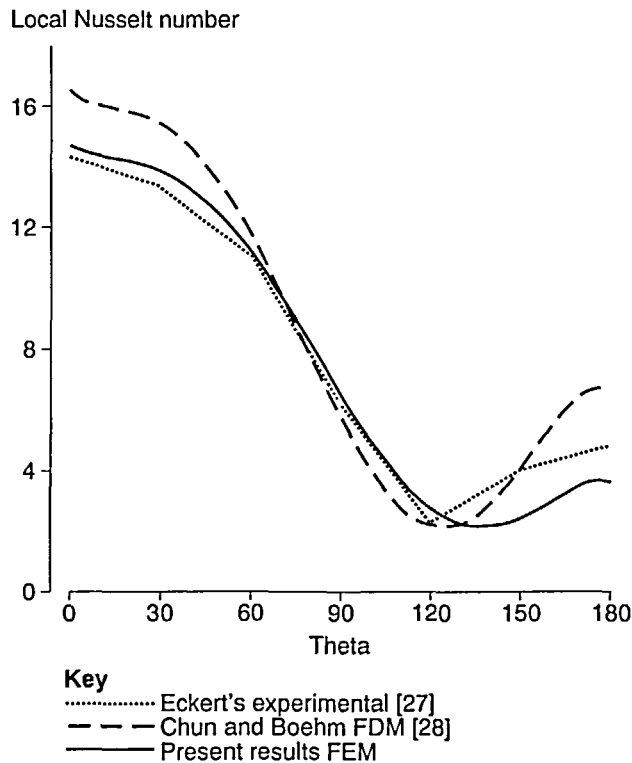— — — Chun and Boehm FDM [28]
————— Present results FEM

Figure 8   Comparison of local Nusselt number distribution at *Re* = 200

starts at the forward stagnation point, the thermal resistance is less in the beginning. Hence, local Nu at the forward stagnation point is higher and decreases up to the point of separation. In the wake region beyond the point of separation, a further increase can be seen because of good mixing. The present finite element results compare well with the experimental values up to the point of separation.

VORTEX SHEDDING FROM CYLINDER WITH SPLITTER

When flow takes place past a circular cylinder with splitter at *Re* = 200 and *BR* = 0.25, in the initial stages of flow irrespective of splitter length and configuration, two attached standing eddies are formed. These eddies grow in size with time and are subsequently shed. The time period of vortex shedding is precisely obtained by monitoring the velocity of signal traces in the downstream. The time history of monitored velocity for a rectangular splitter of length 0.25D, attached to the cylinder at *BR* = 0.25 and *Re* = 200, can be seen in *Figure 9(a)* and *9(b)*. The two monitored points gave the same time period of shedding "T_{ps}". The time period for half shedding cycle can visually be noticed in terms of eddy reversal from top to bottom as in *Figure 10*. In the figure, apart from the serpentine motion in the downstream, another eddy, formed on the opposite side and about to get washed away in the wake, can be seen. *Figure 11* shows the Kärmän vortex street in terms of isovorticity contours for the case of a triangular IWSP of 0.5D length. Here the convection of vortices in the downstream can be noticed.
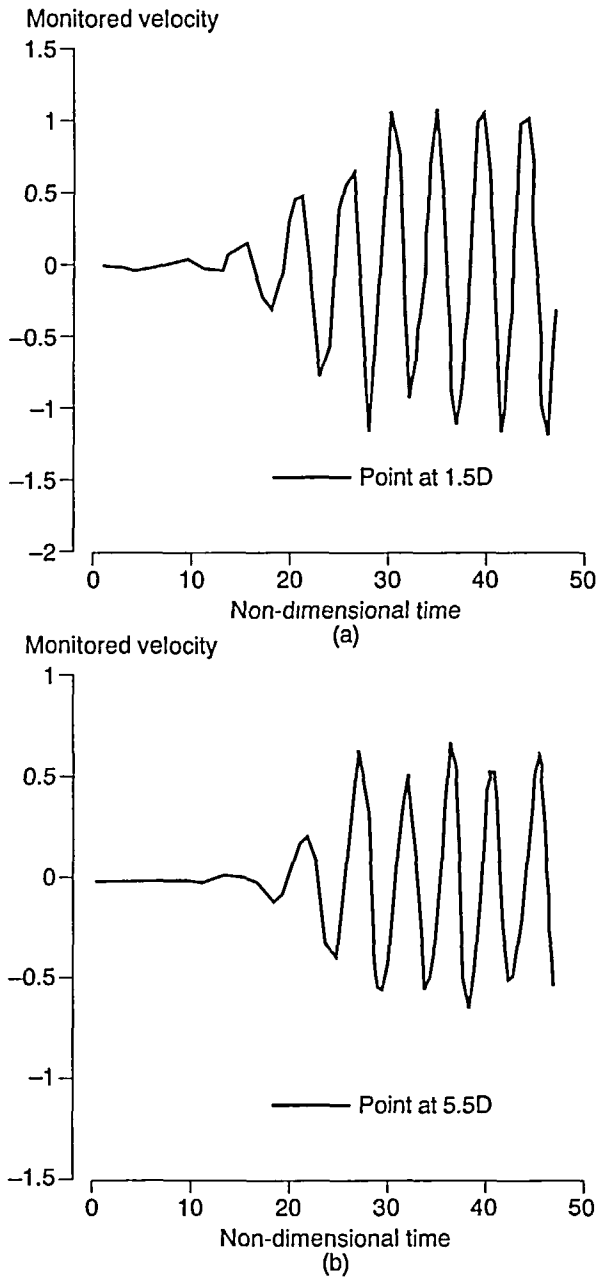
Figure 9   Time history of monitored velocity at two points which show the same time period. (a) Point monitored at 1.5D downstream; (b) Point monitored at 5.5D downstream

EFFECT OF SPLITTER ADDITION ON STROUHAL NUMBER

The effect of time period of shedding "T_{ps}" and Strouhal number "St" are shown in *Figure 12(a)* and *12(b)* for rectangular and triangular IWSPs respectively. For a rectangular IWSP with increase in the length of the splitter, the time period of shedding (i.e. for two vortices to shed, one
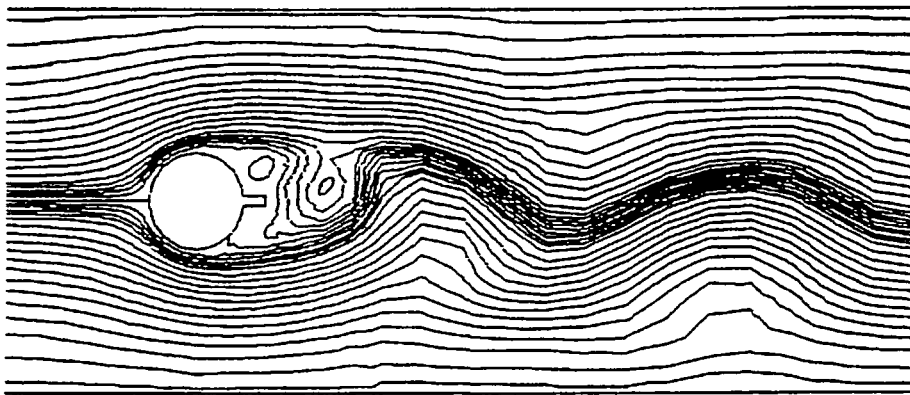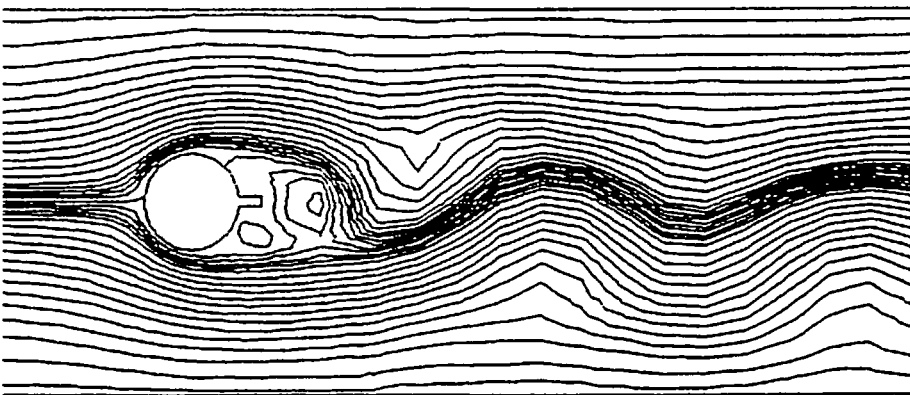
(a) Time = 30.2; *Re* = 200; SPL *L/D* = 0.25

(b) Time = 32.3; *Re* = 200; SPL *L/D* = 0.25

Figure 10   Streamlines half shedding cycle apart. *L/D* = 0.25; *BR* = 0.25 and *Re* = 200. (a) Eddy at the top;
(b) Eddy at the bottom

from the top and another from the bottom) is found to increase, resulting in a smaller vortex shedding frequency and, hence, a lower Strouhal number. With increase in rectangular splitter length, *St* decreases. It has been observed in Patnaik[29] that flow past a bluffer body (square cylinder) results in a smaller Strouhal number. The addition of rectangular IWSP makes the arrangement tend to be more bluffer. Also the Strouhal number decrease is because of the increase in length of the eddy formation region. When a splitter plate is attached, it takes longer for the eddy to roll up, as the flow has to take a physically longer path. Hence, the eddy shedding sets up less easily and takes a longer time period. Gerrard[15], in his experiments on cylinders with splitters in the *Re* ranges of 10^3 to 5×10^4, points out that the production of circulation at the rear of the cylinder will increase.

Interestingly, triangular splitter addition gave a contrasting trend as in *Figure 12(b)*. For a splitter length of 0.25D the shedding period decreased to 3.8 and for 0.5D this period is increased to 4.2. But for a splitter length of 1D the time period of shedding decreased to 3.9. When a triangular IWSP is attached, the body can be considered to be less bluffer. This possibly resulted in a faster shedding of the vortices which influenced in a lesser time period of shedding and higher Strouhal number (when compared to rectangular IWSPs). It should be mentioned that for an elliptic cylinder, which is a less bluffer body, the Strouhal number is higher, in comparison to a circular cylinder.
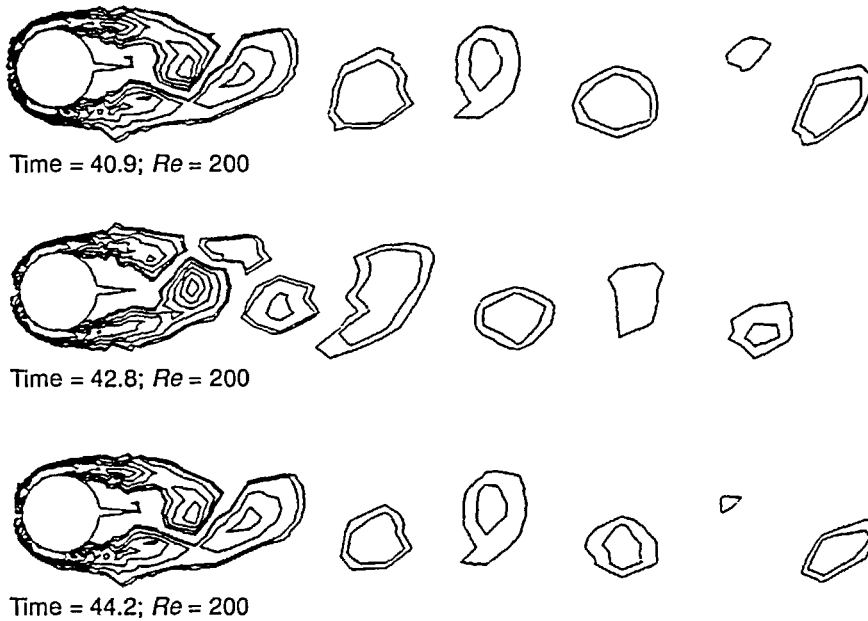
Time = 40.9; *Re* = 200

Time = 42.8; *Re* = 200

Time = 44.2; *Re* = 200

Figure 11   Kàrmän vortex street for *Re* = 200 in one shedding cycle *BR* = 0.25 and *Re* = 200

PRESSURE DISTRIBUTION

The distribution of pressure coefficient on the cylinder with splitter has been compared with that of the cylinder without splitter in *Figure 13*. The base pressures for the cylinder with a splitter length of 0.5D is –0.7 and for a splitter length of 1.0D it is –0.5. On the contrary, in the case of cylinder without any splitter, the value is –0.8. This clearly shows a higher base pressure with increase in splitter length. This means a higher pressure recovery. The curves are integrated to get the actual pressure drop across the arrangement. Apelt and West[16] have also concluded in their experiments on wake splitters in sub-critical *Re* ranges, that maximum change in base pressure coefficient (C_{PB}) is 50% for $L/D = 1.0$.

HEAT TRANSFER ASPECTS

When the splitter plate is integral with the cylinder, temperature drop takes place along the splitter plate. The heat-transfer coefficient on the splitter surface is specified while solving the Energy equation. The effect of local Nusselt number distribution on the cylinder and splitter surface is shown for a cylinder with rectangular splitter in *Figure 14* for $Pr = 0.72$, which corresponds to air. With the splitter addition, the minimum local Nusselt number is at the free end of the splitter plate. The thermal boundary layer growth on the body in itself offers an explanation for this local *Nu* minimum. *Table 2* shows the average Nusselt number to be almost a constant value.

HEAT TRANSFER AUGMENTATION

The average Nusselt number per unit pressure drop has been plotted against the splitter length in *Figure 15*. For a Prandtl number of 0.72, there is a clear heat transfer augmentation for both rectangular and triangular splitters up to a splitter length of 0.5D. This is possible because of
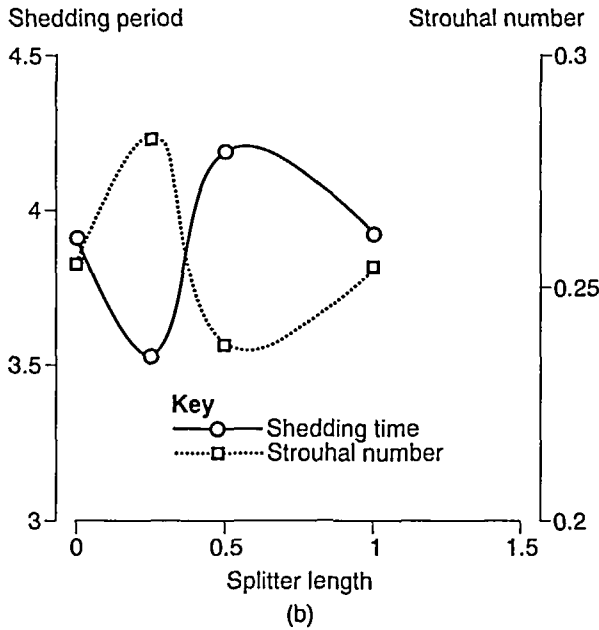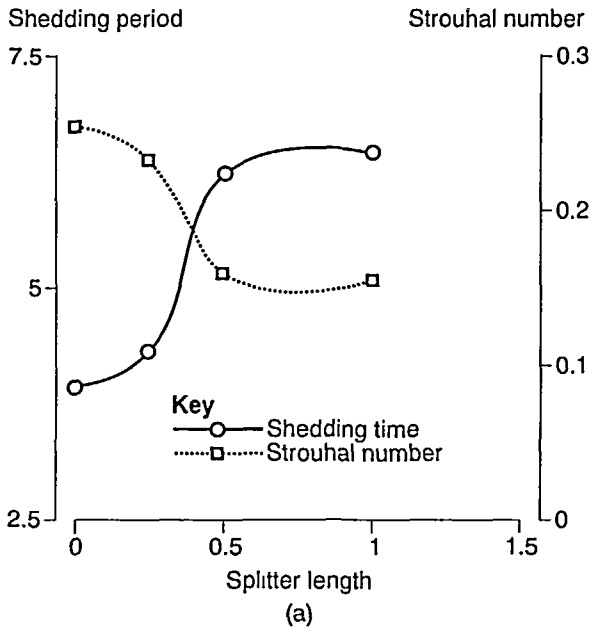
Figure 12   Variation of Strouhal number and time period of shedding with splitter length at $Re = 200$ and $BR = 0.25$.
(a) Rectangular splitter plate; (b) Triangular splitter plate

smaller form drag with splitter addition. Though the average Nusselt number remained almost constant irrespective of the presence of the splitter, the base pressure recovery resulted in the decrease in pressure drop with splitter addition.
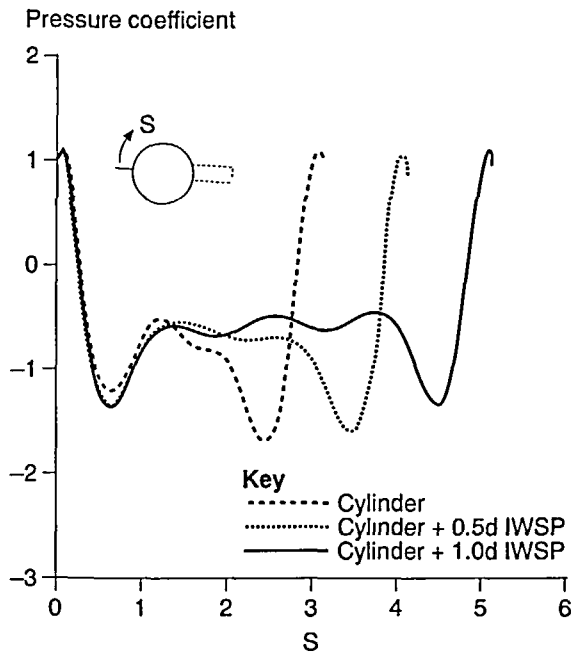
Pressure coefficient

Figure 13   The effect of triangular IWSP on pressure distribution at Re = 200 and BR = 0.25
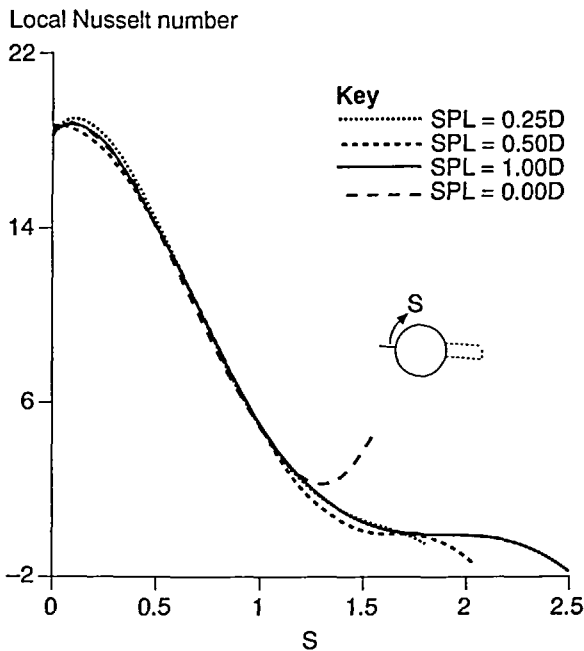
Local Nusselt number

Figure 14   Local Nusselt number distribution for the cylinder with rectangular splitter

Table 2   Average Nusselt number variation for air $Pr = 0.72$, for the two splitter configurations

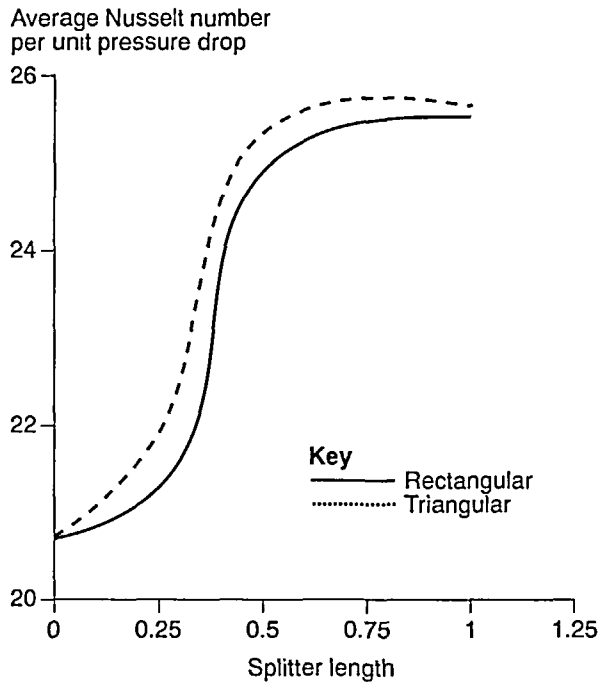| Configuration type	Length of the splitter (L/D)			
	0.0	0.25	0.5	1.0
Rectangular	9 67	9.47	9.42	9.33
Triangular	9.67	9.52	9.56	9.37

Figure 15   Heat transfer augmentation with splitter length at $Re = 200$, $BR = 0.25$ and $Pr = 0.72$

CONCLUSIONS

For a Reynolds number of 200 at a blockage ratio of 0.25, the vortex shedding process is numerically simulated behind a circular cylinder and also with the splitter addition. The phenomenon resulting from the instantaneous "alley-way" concept has been presented, and the underlying flow physics is clearly brought out by means of streamlines and isovorticity contours.

The time period of shedding has been precisely obtained, by monitoring the signal traces of velocity in the Y-direction, from which the Strouhal number has been calculated.

The time period of vortex shedding increased with the rectangular splitter length. However, the triangular splitters make the body to be less bluffer and resulted in a reduction in the time period of shedding.

The average Nusselt number is almost constant for various splitter lengths. However, there is an increase in base pressure recovery. Thus the overall pressure drop is found to decrease. This leads to an increase in the average Nusselt number per unit pressure drop. Hence, heat transfer augmentation per unit pressure drop is achieved with the addition of wake splitter.

ACKNOWLEDGEMENTS

REFERENCES

1   Blevins, R.D., *Flow Induced Vibrations,* Von Nostrand Reinhold, New York, NY (1983)
2   Zadrakovich, M.M., Smoke observations of a Kärmàn vortex street, *J. Fluid. Mech.,* **39**, 491-511 (1969)
3   Aref, M. and Siggia, E.D , Evolution and break down of a vortex street in two dimensoions, *J. Fluid Mech.,* **109**, 435-463 (1981)
4   Perry, A E., Chong, M.S. and Lim, T.J., The vortex shedding process behind two-dimensional bluff bodies, *J. Fluid Mech.,* **116**, 77-90 (1982)
5   Gresho, P.M., Chan, S.T., Lee, R.L. and Upson, C.D., A modified finite element method for solving the time-dependent incompressible Navier-Stokes equations Part II: applications, *Int. J. Numer. Method. Fluids,* **4**, 619-640 (1984)
6   Sa, J.Y. and Chang, K.S., Shedding patterns of near wake vortices behind a circular cylinder, *Int. J. Numer. Method. Fluids,* **12**, 463-474 (1991)
7   Kelkar, K.M. and Patankar, S.V., Numerical prediction of vortex shedding behind a square cylinder, *Int. J. Numer. Method. Fluids,* **14**, 327-341 (1992)
8   Ökajima, A., Strouhal number of rectangular cylinders, *J. Fluid. Mech.,* **123**, 379-398 (1982)
9   Mukhopadhyay, A., Biswas, G. and Sundararajan, T., Numerical investigation of confined wakes behind a square cylinder in a channel, *Int. J. Numer. Method. Fluids,* **14**, 1473-1484 (1992)
10 Slaouti, A. and Stansby, P.K., Flow around two circular cylinders by the random-vortex method, *J. Fluids. and Structures,* **6**, 641-670 (1992)
11 Slaouti, A., and Gerrard, J.H., An experimental investigation of the end effects of a circular cylinder towed through water at low Reynolds numbers, *J. Fluid. Mech ,* **112**, 297-314 (1982)
12 Roshko, A., On the wake and drag behind bluff bodies, *J. Aero Sci.,* **22**, 124-132 (1955)
13 Roshko, A., Experiments on the flow past a circular cylinder at very high Reynolds number, *J. Fluid Mech.,* **10**, 345-356 (1960)
14 Bearman, P.W , Investigation of the flow behind a two-dimensional model with a blunt trailing edge and fitted with splitter plates, *J. Fluid. Mech.,* **61** (3), 499-511 (1965)
15 Gerrard, J.H., The mechanics of the formation region of vortices behind bluff bodies, *J. Fluid. Mech.,* **25**, 401-413 (1966)
16 Apelt, C.J. and West, G S., The effect of wake splitter plates on bluff body flows in the range $10^2 < Re < 5 \times 10^4$: Part 2, *J. Fluid Mech.,* **71**, 145-160 (1975)
17 Sparrow, E.M. and Kang, S.S., Longitudinal finned cross flow tube banks and their heat transfer and pressure drop characteristics, *Int. J. Heat Mass Transfer,* **28**(2), 339-350 (1985)
18 Ibrahim, A.M.A., Augmentation of heat transfer in flow over a bank of tubes by integral wake splitter plates, PhD Thesis, Indian Institue of Technology, Madras, India (1990)
19 Chorin, A.J., A numerical method for for solving incompressible viscous flow problems, *J. Comp. Phys.,* **2**, 12-26 (1967)
20 Donea, J., Ginliani, S., Laval, H. and Quartapele, Finite element solution of unsteady Navier-Stokes equations by fractional step method, *Comp. Method. Appl. Mech. Eng.,* **30**, 53-73 (1982)
21 Fletcher, C.A.J., *Computational Galerkin Methods,* Springer-Verlag, New York, (1984)
22 Segarlind, L.J., *Applied Finite Element Analysis,* John Wiley, New York, (1984)
23 Mukhopadhyay, A., A calculation procedure for viscous incompressible flows in arbitrary geometry and confined wakes behind partially enclosed bluff bodies, PhD Thesis, Dept. Mechanical Engg, IIT, Kanpur (1992)
24 Son, J.S. and Hanratty, T.J., Numerical flow around a cylinder at Reynolds numbers of 40, 200 and 500, *J. Fluid Mech.,* **35**(2), 369-386 (1969)
25 Braza, M., Chassiang, P. and Ha Minh, M., Numerical study and physical analysis of pressure and velocity field in the near wake of a circular cylinder, *J. Fluid. Mech.,* **165**, 79-130 (1983)
26 Karniadakis, G.M., Numerical simulation of forced convection heat transfer from a cylinder in cross flow, *Int. J. Heat Mass Transfer,* **31**(1), 107-118 (1988)
27 Eckert, E.R.G. and Soehngen, E., Distribution of heat transfer coefficient around circular cylinders in cross flow at Reynolds numbers from 20 to 500, *Trans. ASME, J. Heat Trans.,* **74**, 343-347 (1952)
28 Chun, W. and Boehm, R.F., Calculation of forced flow and heat transfer around a circular cylinder, *Numer. Heat Mass Trans.,* **15**, 101-122 (1989)
29 Patnaik, B.S.V.P., Finite element analysis of flow past bluff bodies with heat transfer, MS Thesis, Indian Institute of Technology, Madras, India (1994)

This article has been cited by:

1. M Subhash Reddy, Sridhar Muddada, B S V Patnaik. 2013. Flow past a circular cylinder with momentum injection: optimal control cylinder design. *Fluid Dynamics Research* **45**:1, 015501. [CrossRef]

2. Chennu Ranganayakulu, Jaideep S. Mathur and Perumal NithiarasuRajesh SahuDepartment of Applied Mechanics, Indian Institute of Technology Madras, Chennai, India B.S.V. PatnaikDepartment of Applied Mechanics, Indian Institute of Technology Madras, Chennai, India. 2011. CFD simulation of momentum injection control past a streamlined body. *International Journal of Numerical Methods for Heat & Fluid Flow* **21**:8, 980-1001. [Abstract] [Full Text] [PDF]

3. Khyati Varma, Hui Hu, Zhi WangNumerical Simulation of Effects of Buoyancy on Wake Instability of Heated Cylinder In Contra Flow . [CrossRef]

4. S. Tiwari, D. Chakraborty, G. Biswas, P.K. Panigrahi. 2005. Numerical prediction of flow and heat transfer in a channel in the presence of a built-in circular tube with and without an integral wake splitter. *International Journal of Heat and Mass Transfer* **48**:2, 439-453. [CrossRef]

5. K Murugesan, H.N Suresh, K.N Seetharamu, P.A Aswatha Narayana, T Sundararajan. 2001. A theoretical model of brick drying as a conjugate problem. *International Journal of Heat and Mass Transfer* **44**:21, 4075-4086. [CrossRef]

6. B. S. Varaprasad Patnaik, Y. T. K. Gowda, M. S. Ravisankar, P. A. Aswatha Narayana, K. N. Seetharamu. 2001. Finite element simulation of internal flows with heat transfer using a velocity correction approach. *Sadhana* **26**:3, 251-283. [CrossRef]

7. B.S.V. PatnaikDepartment of Computational Science, NUS, Singapore P.A.A. NarayanaDepartment of Applied Mechanics, IIT, Madras, India, and K.N. SeetharamuDepartment of Mechanical Engineering, USM, Perak, Malaysia. 2000. Finite element simulation of transient laminar flow past a circular cylinder and two cylinders in tandem – Influence of buoyancy. *International Journal of Numerical Methods for Heat & Fluid Flow* **10**:6, 560-580. [Abstract] [Full Text] [PDF]

8. K. Murugesan, K. N. Seetharamu, P. A. Aswatha Narayana, H. R. Thomas, W. J. Ferguson. 2000. Study of shrinkage stresses for drying of brick as a conjugate problem. *International Journal for Numerical Methods in Engineering* **48**:1, 37-53. [CrossRef]

9. E.R.G. Eckert, R.J. Goldstein, W.E. Ibele, T.W. Simon, T.H. Kuehn, P.J. Strykowski, K.K. Tamma, A. Bar-Cohen, J.V.R. Heberlein, J.H. Davidson, J. Bischof, F. Kulacki, U. Kortshagen. 2000. Heat transfer — a review of 1996 literature. *International Journal of Heat and Mass Transfer* **43**:8, 1273-1371. [CrossRef]

10. B.S VARAPRASAD PATNAIK, P.A ASWATHA NARAYANA, K.N SEETHARAMU. 1999. NUMERICAL SIMULATION OF LAMINAR FLOW PAST A TRANSVERSELY VIBRATING CIRCULAR CYLINDER. *Journal of Sound and Vibration* **228**:3, 459-475. [CrossRef]

11. B.S. Varaprasad Patnaik, P.A. Aswatha Narayana, K.N. Seetharamu. 1999. Numerical simulation of vortex shedding past a circular cylinder under the influence of buoyancy. *International Journal of Heat and Mass Transfer* **42**:18, 3495-3507. [CrossRef]

12. Y.T Krishne Gowda, B.S.V.P Patnaik, P.A Aswatha Narayana, K.N Seetharamu. 1998. Finite element simulation of transient laminar flow and heat transfer past an in-line tube bank. *International Journal of Heat and Fluid Flow* **19**:1, 49-55. [CrossRef]